Femtosecond nonlinear absorption of gold nanoshells at surface plasmon resonance. Phys. Chem. Chem. Phys. 12, 13692–13698

ARTICLE *in* PHYSICAL CHEMISTRY CHEMICAL PHYSICS · NOVEMBER 2010

Impact Factor: 4.49 · DOI: 10.1039/c0cp00783h · Source: PubMed

5 AUTHORS, INCLUDING:

Ida Ros
University of Padova
5 PUBLICATIONS **23** CITATIONS
SEE PROFILE

Piero Schiavuta
Veneto Nanotech
31 PUBLICATIONS **306** CITATIONS
SEE PROFILE

Valentina Bello
University of Padova
63 PUBLICATIONS **694** CITATIONS
SEE PROFILE

Renato Bozio
University of Padova
169 PUBLICATIONS **3,148** CITATIONS
SEE PROFILE

Femtosecond nonlinear absorption of gold nanoshells at surface plasmon resonance

Ida Ros,[a] Piero Schiavuta,[b] Valentina Bello,[c] Giovanni Mattei[c] and Renato Bozio*[a]

Received 3rd June 2010, Accepted 22nd July 2010
DOI: 10.1039/c0cp00783h

The nonlinear optical absorption of gold nanoshells (Au NSs) of different size, in water, was investigated using open aperture *z*-scan technique with femtosecond laser pulses at 806 nm. It is found that, in general, NSs behave as saturable absorbers. The level of saturation depends on the Au NSs structure and precisely on the ratio between the core size and shell thickness. The measured values of the nonlinear absorption coefficient show a dependence on both the repetition rate and the pulse energy. An average value of the nonlinear absorption coefficient $\beta = -4.5 \pm 1.0 \times 10^{-11}$ cm W^{-1} is obtained from *z*-scan data of core–shell particles of inner and outer radius 95 and 110 nm, respectively, measured at 20 Hz repetition rate in the energy range 120–300 nJ.

Introduction

The ability to control the material properties of nanostructures through careful planning of their size and shape features is very important for device applications.[1–3] For example, noble metal nanoparticles (NPs) have received special attention because of their optical properties. Differing from the broad structureless absorption spectra of the corresponding bulk metals, they show an absorption band in the visible region of the electromagnetic spectrum that depends on the shape, the size, the embedding medium and, obviously, on the metal making up the nanostructures.[4–7] The well defined absorption band is due to a surface plasmon resonance (SPR) and corresponds to the coherent motion of the conduction-band electrons caused by the interaction with the electromagnetic field.

Presently, there is great interest in metal nanoshells (NSs),[8–10] a new type of composite nanoparticles consisting of a dielectric core (silica or polystyrene) coated with a nanometre thick metallic shell, usually gold. Research has focused on NSs because they offer the ability both to move the plasmon resonance anywhere across the visible or infrared regions of the spectrum and to manipulate the relative scattering and absorption efficiencies simply by adjusting the relative size of the dielectric core and the thickness of the gold overlayer. The possibility to tune the resonance wavelength in the near infrared region (NIR), where penetration of light through biological tissues is maximal, is very appealing for applications in biomedicine, including photothermal cancer therapy,[11] immunoassays, and imaging contrast agents.[9] Other interesting applications are in the field of sensing and single molecule detection (SERS,[12] SEIRA).[13] NSs are also of interest because they can be exploited to amplify the local field in the near-infrared and to increase the efficiency of nonlinear (NL) processes, such as second harmonic generation and two-photon absorption,[14] of molecules or polymers functionalizing NSs. To this aim, it is important to investigate the intrinsic nonlinear optical (NLO) properties of NSs in order to gain the background knowledge needed for understanding the behavior of functionalized nanoparticles.

Currently, NLO properties of noble metal NPs in solution[15–19] and embedded in a glass matrix[20–23] have been investigated by the open aperture *z*-scan technique because of their large third-order susceptibility and the ultrafast response times. In general, when excited near the SPR band, metal NPs behave as a saturable absorbers owing to the bleaching of the ground-state plasmon band. In some cases, at higher pump intensity, gold nanorods,[15] platinum[17] and silver[22] NPs change their behavior from saturable absorber to reverse saturable absorber (*i.e.*, absorption increases at high input intensities) due to free carrier absorption.

Open aperture *z*-scan measurements can be performed either under one-photon resonant conditions or by shining light in a transparent region of the material. In the latter case, the data provide information on instantaneous two- or multi-photon absorption processes. Metal nanostructures have been excited by 532 nm nanosecond and picosecond laser pulses (gold, silver and platinum NPs) or 805 nm femtoseconds laser pulses (gold nanorods and twin linked gold NPs), depending on the SPR band wavelength. By fitting the experimental results, it is possible to obtain the nonlinear absorption coefficient; the data obtained are strongly dependent on the experimental conditions (nature of the sample as well as pulse characteristics).[24]

Very different nonlinearity values are published for gold nanoparticles,[18,20,22,23,25] from -10^{-2} cm W^{-1} for gold nanorods in a silica matrix excited by a 22 ns pulses at 532 nm,[25] to -10^{-10} cm W^{-1} for gold nanoparticles in water excited by 30 ps pulses at 532 nm.[18]

In this work, we present an investigation of the NLO properties of gold NSs of different size in solutions using a single beam *z*-scan method at a wavelength of 806 nm with laser duration of 170 fs. To the best of our knowledge,

[a] *Department of Chemical Sciences and INSTM, University of Padova, via Marzolo 1, 35131, Padova, Italy. E-mail: renato.bozio@unipd.it*
[b] *Nano Fabrication Facility, via delle Industrie 9, 30175, Venezia-Marghera, Italy*
[c] *CNISM and Department of Physics, University of Padova, via Marzolo 8, 35131 Padova, Italy*

this is the first time that NLO properties of NSs have been investigated. Beside using a carefully chosen pulse energy range in order to control the reshaping and avoid the destruction of the metallic shell,[26,27] we also checked the effect of varying the pulse repetition rate in order to minimize thermal effects due to pulse-to-pulse accumulation of the deposited energy. In all our measurements, NSs suspensions behave as saturable absorbers, the level of saturation depending on the relative overlap between the plasmon resonance of NSs and the laser excitation wavelength.

An effective value of the NL absorption coefficient β ranging between -1.1×10^{-11} cm W^{-1} and -9.6×10^{-11} cm W^{-1}, dependent on the pulse energy and repetition rate, is obtained by fitting the experimental results for core–shell particles exhibiting a surface plasmon resonance at different wavelengths.

Materials and methods

Materials

All reagents were used as purchased without further purification: tetraethyl orthosilicate (TEOS), tetrakis(hydroxymethyl)phosphonium chloride (THPC, 80% solution in H_2O), hydrogen tetrachloroaurate-(III) hydrate, potassium carbonate were from Sigma-Aldrich; polyvinylpyrrolidone (PVP, MW 40 000), 3-aminopropyltrimethoxysilane (APTMS), ammonium hydroxide and formaldehyde were from Fluka; sodium hydroxide was from Carlo Erba. Similarly, all solvents were used as received: toluene (Aldrich) and absolute ethanol (J.T. Baker); deionized water (18 MΩ) was provided by a Milli-Q system.

Nanoshells fabrication

The synthesis of NSs (SiO_2@Au) is a multi-step process realized in water following the procedure developed by Pham *et al.*[28] Briefly, silica particles of about 100–200 nm in diameter are prepared *via* the Stöber method[29] and functionalized with APTMS. These molecules, extending their amine groups outward as a new termination of the nanoparticle surface, act as a binding site for small colloidal gold particles (of about 2 nm dia.) prepared separately.[30] Finally, the gold-decorated silica nanoparticles are used as nucleation sites for the reduction of an aged mixture of chloroauric acid and potassium carbonate (growth solution) by an aliquot of formaldehyde. Nanoshells are stabilized by adding some PVP to the solution.

By varying the ratio between the growth solution and the amount of gold-decorated silica particles, we achieve different thickness of the shell covering the core surface. As the amount of silica nanoparticles decreases, keeping the volume of the growth solution constant, gold is first reduced onto the colloidal adsorbates, subsequently the nucleation sites grow and begin to coalesce and form islands before achieving full coverage of the shell.

Two different size NSs are prepared: one with 50 nm inner radius (R_1) and 10 nm shell thickness and one with $R_1 = 95$ nm and 15 nm shell thickness.

Deposition of nanoshells onto glass slides

Gold NSs were deposited onto glass substrates to measure their morphology. In order to prevent particle movements during the AFM characterizations, glass substrates were functionalized with APTMS.[31]

All substrates were cleaned prior to silanization. The cleaning process involves a sequential sonication in different solvents: 10 min in deionised water, 10 min in acetone, 10 min in isopropyl alcohol, 10 min in acetone and finally, 10 min in deionised water again.

APTMS monolayers were formed by dipping a sodalime glass into a 1 vol% solution in ethanol for 1 h. Then the substrate was rinsed by sonication in toluene for 40 s. This process of dipping and sonication was repeated a second time to ensure full monolayer coverage.

Silanized substrates were characterized by contact angle measurements, that confirmed literature values.[32] The contact angle of a freshly silanized surface was $47^\circ \pm 2^\circ$, but aging the sample in closed polypropylene vials (in air) caused an increase of the angle value to $64^\circ \pm 3^\circ$.

The substrates were immersed in the NSs solution for $\sim$12 h, then rinsed with water to remove an excess of NSs and finally dried by N_2 flow.

Instrumentation and measurement methods

Structural and compositional characterization was performed by transmission electron microscopy (TEM) at CNR-IMM (Bologna, Italy) with a field-emission gun (FEG) microscope (FEI Tecnai F20 Super Twin) operating at 200 kV equipped with an EDAX energy-dispersive X-ray spectrometer (EDS) and a Gatan STEM controller for performing scanning transmission microscopy (STEM).

Atomic force microscopy (AFM) was performed with a NT-MDT (NT-MDT-Europe B.V., Nuenen, the Netherlands) operating in air in the semi-contact mode with a 3-μm scanner. The probe has a typical curvature radius of 10 nm, a cantilever resonant frequency of 200 kHz, and a force constant of 5.5 N m^{-1}.

UV-vis spectra were collected using a Varian CARY 5 Scan UV-Visible spectrometer over the range from 175 to 3300 nm. All samples were dispersed in water and loaded into a quartz cell for analysis.

The NLO properties of gold NSs in solution were measured by the open aperture *z*-scan technique.[33] The laser source was an amplified regenerative Ti:sapphire system delivering 170-fs-long pulses centered at 806 nm with a repetition rate of 20 or 200 Hz. Typical pulse energies, after suitable attenuation, were in the range 0.1–0.6 μJ.

Results and discussion

Structural and morphological data of deposited films

Two different NSs samples, deposited on glass substrates, are characterized by AFM: $R_1 = 50 \pm 10$ nm, $R_2 = 60 \pm 20$ nm (Fig. 1); $R_1 = 95 \pm 4$ nm, $R_2 = 110 \pm 4$ nm (Fig. 2).

Shells grown on larger cores are more regular: the particles present spherical shape and homogeneous size distribution.

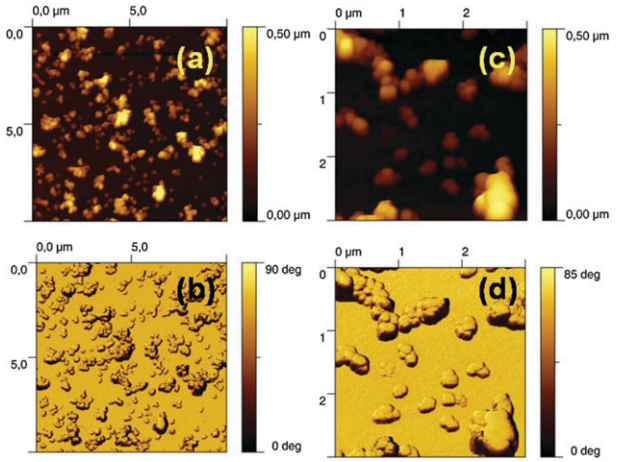

Fig. 1 AFM images of SiO_2/Au nanoshells with R_1 = 50 nm and R_2 = 60 nm on functionalized glass substrate: topography (a) and phase contrast (b) 10 × 10 µm^2 size scan; topography (c) and phase contrast (d) 3 × 3 µm^2 size scan.

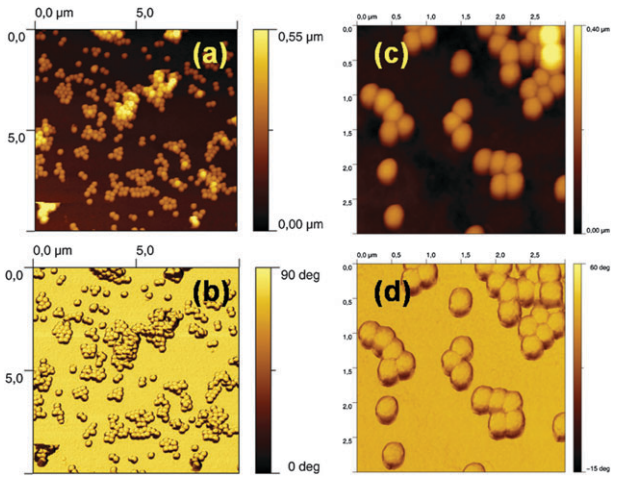

Fig. 2 AFM images of SiO_2/Au nanoshells with R_1 = 95 nm, R_2 = 110 nm on functionalized glass substrate: topography (a) and phase contrast (b) 10 × 10 µm^2 size scan; topography (c) and phase contrast (d) 3 × 3 µm^2 size scan.

Smaller particles present an irregular shell composed of larger domains, for these particles it is quite difficult to define a shell thickness because of the irregularity, so the error bar is rather large. The surface morphology of a single particle influences the NSs aggregation. Particles covered by an irregular shell aggregate randomly. Instead, more regular particles self-assemble in a hexagonal close-packed structure.

Nanoshells with $R_1 = 95 \pm 4$ nm $R_2 = 110 \pm 4$ nm were also characterized by TEM, to confirm results obtained by AFM. A TEM bright-field (BF) micrograph of the SiO_2 particles is shown in Fig. 3a: the silica NPs exhibit a mean diameter $\langle D \rangle$ = 167 nm with a standard deviation of the size distribution σ = 12 nm (see Fig. 3b), *i.e.* corresponding to an average NP radius $R_{TEM} = 84 \pm 6$ nm. The atomic ratio O/Si, found by EDS compositional analysis, is about 2.2 ± 0.2. This can be an indication of a slightly less dense silica, as sometimes it is found for the Stöber synthesis.

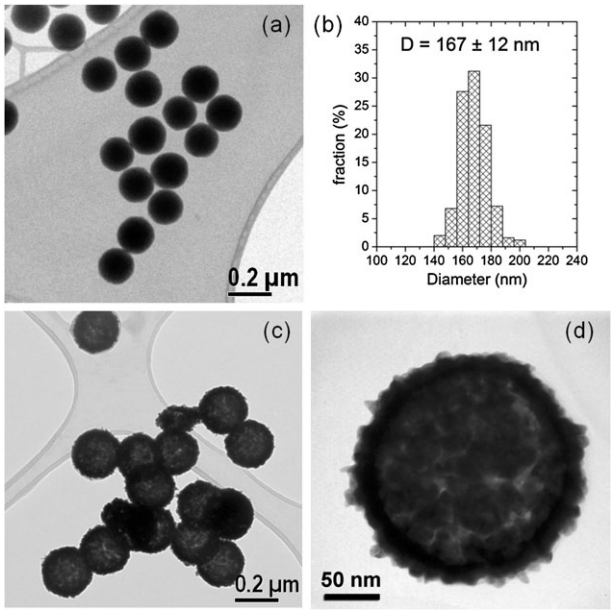

Fig. 3 TEM results on SiO_2 NPs and the SiO_2/Au NSs deposited on a carbon film: (a) BF-TEM image of the SiO_2 NPs; (b) the corresponding size distribution; (c) BF-TEM image of the SiO_2/Au NSs; (d) higher magnification on a single NS.

The silica core radius measured by AFM is slightly larger than the one measured by TEM: this 10% discrepancy can be ascribed to the different spatial resolution and sensitivity of the two techniques but also to a possible shrinking effect of the not-fully densified NPs under the TEM electron beam.[34] Fig. 3c and d show the BF-TEM images of SiO_2/Au core–shell particles with a spherical shape and a mean diameter $\langle D \rangle$ = 220 nm with a standard deviation of the size distribution σ = 15 nm, perfectly comparable with the value obtained by AFM. Few smaller or irregularly shaped NSs are also visible in Fig. 3c. The contrast analysis of the TEM image indicates that the Au shell covering the SiO_2 particles is not continuous, *i.e.*, its thickness is not homogeneous. Moreover, some NSs appear surrounded by a thin PVP film (Fig. 3d), which likely condensate on the NS during solvent evaporation after depositing the NS on the TEM supporting grid.

HR-TEM analysis (not shown) confirmed that the Au shell is polycrystalline, as can be expected from the colloidal-nucleated growth of the fabrication process. The Au surface appears very rough or bumpy. Therefore the definition of the size has been done by radially averaging the image intensity, so as to average the roughness effect. By difference, the resulting thickness of the Au shell t_{shell}, which is the main parameter triggering the optical properties of the NSs, can be estimated as $t_{shell} = (26 \pm 10)$ nm. To check the validity of this approach we calculated also the shell thickness by EDX analysis. Indeed, integrating the X-ray signal over the entire NS, an atomic ratio Au/Si = 3.5 ± 0.5 is found. So, considering an ideal core–shell particle (with a continuous Au shell homogeneously covering a SiO_2 core of diameter $\langle D \rangle = (167 \pm 12)$ nm), and assuming the bulk density for Au and a 10% less dense SiO_2 with respect to the bulk value, the volume occupied by Au (*i.e.*, the shell)

results to have an average thickness t_{shell} = (25 ± 5) nm, in good agreement with the previous one.

Extinction spectra of solutions

Extinction spectra of silica–gold NSs in water with different inner (R_1) and outer (R_2) radius (*i.e.*, R_1 = 50 nm, R_2 = 60 nm; R_1 = 95 nm, R_2 = 110 nm) are shown in Fig. 4.

All the spectra are characterized by a broad plasmon peak with a broad shoulder at longer wavelength. As described previously,[13,35] the peak broadening of the spectra can arise from: (1) the polydispersity of the core particles;[36] (2) the roughness of the shell surfaces; (3) the presence of particles with incomplete shell;[26] (4) the overlap of multipole surface plasmon resonances (*e.g.*, quadrupole and octupole) arising from the large NS particles; (5) particle aggregation.

Considering the morphological characterization shown in section 3.1 and the typical models used in the literature to describe the plasmon resonances of core–shell structures,[4,5] it is clear that NSs with an incomplete coverage full of apexes do not possess a narrow band and their extinction spectra cannot be predicted by these models. Recently, Preston *et al.*,[37] using the discrete dipole approximation, have found that the plasmon modes of incomplete gold layers on silica particles exhibit two bands: one from 500–600 nm ("high energy") and the other from 600–800 nm ("low energy"). A similar shape is found in the spectra of NSs with an inner core of 95 nm. The two bands are red shifted probably due to the effect of the tips. Clearly, a more detailed analysis is needed to determine a model that completely describes the extinction spectra.

A volume fill fraction of the order of 10^{-5} is obtained, based on geometrical considerations, for both NSs suspensions. At this low value, we can consider non-interacting particles and we can neglect their mutual interaction.

z-Scan measurements

Through the *z*-scan technique, it is possible to measure characteristic constants associated with NLO phenomena (*i.e.* NL refractive index and NL absorption coefficient) simply measuring variations in transmittance. A laser beam is focused by a lens of suitable focal length onto a sample mounted on a translation stage. The stage is moved around the focal region along the beam propagation direction (*Z* axis) from the side of the detector toward that of the focal lens (negative values of *Z* correspond to locations of the sample between the focusing lens and its focal plane, positive values correspond to the sample positioned between the detector and the focal plane). Starting the scan from a distance far away from the focus, the beam irradiance is low and NLO effects are negligible; hence, the transmittance remains rather constant. As the sample is brought closer to the focus, the beam irradiance increases, leading to sizeable NLO phenomena.

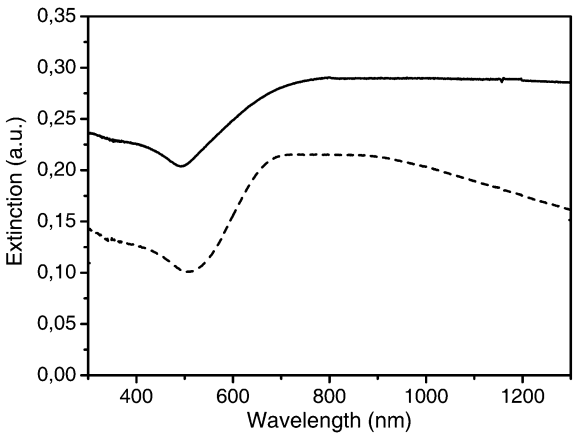

Fig. 4 Extinction spectra of nanoshells suspension: R_1 = 50 nm, R_2 = 60 nm (full line), R_1 = 95 nm, R_2 = 110 nm (dash line).

In this work, the open aperture *z*-scan method is used to measure the intensity-dependent NL absorption coefficient β. The normalized transmittance can be expressed as[33]

$$T_{\mathrm{Norm}}(z) = \sum_{m=0}^{\infty} \left[\left(\frac{-\beta I_0 L_{\mathrm{eff}}}{1 + z^2/z_0^2} \right)^m \Big/ (1+m)^{3/2} \right] \qquad (1)$$

where β is the NL absorption coefficient, $L_{\mathrm{eff}} = (1 - e^{\alpha_0 L})/\alpha_0$ is the effective interaction length with the sample thickness L, and α_0 is the linear absorption coefficient. Typically, if $|\beta I_0 L_{\mathrm{eff}}|$ is small compered to one, only the first few terms are needed for numerical simulation. Thus β can be determined from a fit of eqn (1) to the experimental results.

Although *z*-scan is a very simple technique, it presents some limitations in measuring NLO properties of metal nanoparticles and other materials in general. First of all, the absorption by the sample of a laser pulse train can cause heating of the sample. Thermal phenomena may mask electronic properties of the material since they can produce very intense non-linearities. It is thus necessary to work with short pulses, for example femtosecond pulses instead of nanosecond ones, at low repetition rates to reduce thermal effects. The second limitation is due to the fact that the time scale of the experiment is set by the pulse duration. Transient phenomena that die out too quickly may at most reach a steady state that is too weak to detect. On the other hand, phenomena occurring on a time scale much longer than the pulse width do not have time to set in. Therefore, *z*-scan experiments provide an effective measurement of the NLO response dominated by phenomena occurring on the same time scale as the duration of the laser pulse employed.

As shown in Fig. 5, all the NSs suspension samples behave as saturable absorbers at both 20 and 200 Hz repetition rate and in all the range of pulse energies employed. The amplitude of the saturation signal increases with energy at both repetition rates. However, a peculiar phenomenon is observed on increasing energy and/or repetition rate: the saturation peak becomes increasingly asymmetric. Comparing the *z*-scan traces for the same sample at the same energies but at different repetition rates, saturation is larger at 200 Hz. This is probably due to thermal effects. The NSs size influences the femtosecond laser pulse response. Although the UV-visible spectra are broad and it is quite difficult to locate a unique or a central wavelength of the surface plasmon resonance, the saturation is clearly enhanced for NSs with R_2 = 110 nm. These NSs are, in fact, characterized by a plasmon that is more resonant with the laser wavelength at 806 nm. For example, comparing, in

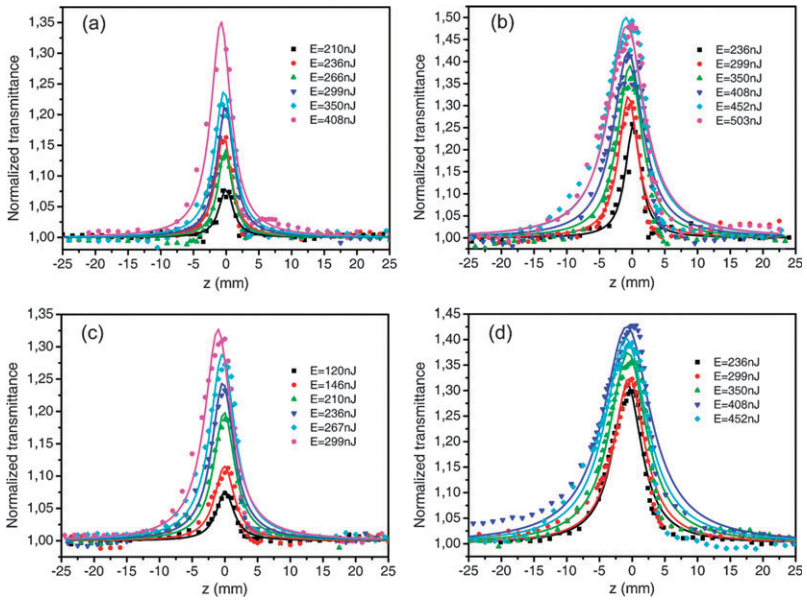

Fig. 5 Open-aperture *z*-scan measurements at (a) 20 Hz and (b) 200 Hz repetition rate of the gold nanoshells R_2 = 60 nm in solution, (c) 20 Hz and (d) 200 Hz repetition rate of gold nanoshells R_2 = 110 nm in solution. The solid lines indicate a theoretical fit.

Fig. 5, *Z*-scan traces at the same pulse energy (210 nJ) and repetition rate (20 Hz) for NSs with R_2 = 60 nm (black full square) and NSs with R_2 = 110 nm (green full triangle), saturation is 8% for the former and 20% for the latter even if the volume fill fraction of larger NSs is lower than the fill fraction of smaller ones.

The peak asymmetry is made evident by plotting the fit residues for NSs R_2 = 60 nm and R_2 = 110 nm at two energies and both repetition rates (data not shown). The residues show a sigmoidal trend, negative values are associated with calculated values greater than experimental data, and *vice versa*. Increasing energy causes an enlargement of the sigmoid and of the peak-to-peak difference at both the repetition rates.

In Fig. 6 the NLO response of NSs R_2 = 110 nm at the same energy and reversing the direction of the stage motion along the beam (from positive to negative values of *z* or *vice versa*) is shown. The asymmetry reverts on approaching the focal plane either from the side of the laser source or from that of the detector. This effect is made evident by plotting, as an example, the fit residues (Fig. 6b). The sigmoidal trend reverses on reverting the scan direction. This is a clear indication that a residual effect of NL refraction or NL scattering does not contribute to the phenomenon since it would be unaffected by the reversal of the stage motion.

The saturation peak asymmetry is due to a reshaping of the NSs under femtosecond illumination.[26,27] Time diffusion of NSs covered by PVP in water is too long to supply constantly fresh nanoparticles into the illumination area, during *z*-scan measurement. As the sample approaches the focus and the intensity increases, gold nanoshells reshape causing the NLO response changes because they have not enough time to diffuse out of the beam waist. However, the gold coverage is not completely destroyed because the NSs response continues also after reshaping.

UV-visible spectra of NSs, exposed to laser irradiation for times comparable to those used by Aguirre *et al.*,[27] do not change after laser irradiation and apparently, a complete shell is not required to maintain absorption in the near infrared.

Analysis of the *z*-scan curves

The relaxation dynamics of plasma excitations in metallic systems has been investigated extensively.[38–40] Briefly, the laser pulse causes an interband or intraband electron transition in the NS, depending on the excitation wavelength and intensity.

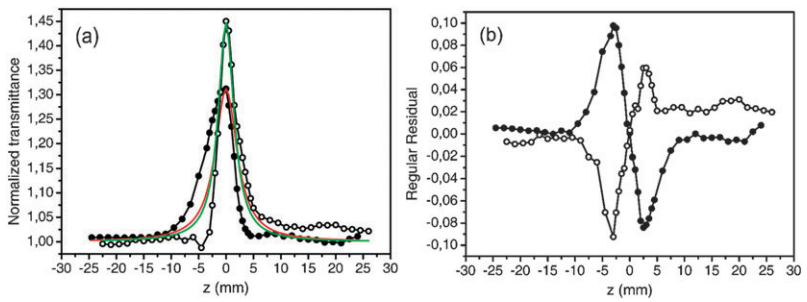

Fig. 6 (a) Open-aperture *z*-scan measurements at 20 Hz repetition rate and (b) fit residual trend of gold nanoshells R_2 = 110 nm in solution, at 299 nJ with regular (black dot) and inverted (empty dot) translation stage motion. The solid lines indicate a theoretical fit.

The electrons, thus excited, have a non equilibrium distribution different from the Fermi–Dirac statistics for fermions.[38] Through electron–electron scattering, the electron gas thermalizes and reaches a new Fermi distribution with a higher electron temperature within 500 fs. After electron thermalization and partly during that process, electrons lose their energy further by thermal equilibration with the lattice through electron–phonon interactions. A thermalization time for the electronic gas through electron–phonon coupling of the order of few ps has been obtained for different size and shape gold nanoparticles. Phonon–phonon relaxation processes follow: thermal energy will be dumped into the solvent causing the dielectric or surrounding medium to change, thereby influencing the plasmon resonance frequency of the NSs.

According to the above analysis, we believe that the *z*-scan results arise from the bleaching of the ground-state plasmon band which leads to saturable absorption. Working with higher energies and repetition rates increases the bleaching effect because more energy is provided to the system and a higher temperature is reached. Within a single fs pulse only the rise in electronic temperature should matter. However accumulation effects at higher repetition rate could cause a small increase of lattice or thermodynamic temperature to become of relevance.

Considering the time scale of the thermalization, we can also explain the asymmetry of the saturable absorption peak, which increases both with energy and repetition rate. In the literature the reshaping effect and disruption of NSs by femtosecond pulsed laser irradiation is well known.[26,27] Depending on the laser pulse energy, on the radiation exposure time and on the shell thickness, it is possible to make a hole in the shell, to completely melt it and produce gold nanoparticles or even to remove the dielectric silica core. During *z*-scan measurements, as the sample is brought closer to focus, the beam irradiance increases and the shell reshapes but is not completely destroyed by pulses in the range of energy we have used, as shown by the fact that the system continues to behave as a saturable absorber.

The results of the fitting by the Sheik–Bahae model yield β values in the order of -10^{-11} cm W^{-1} but they exhibit a significant dependence on the size of the NSs and on the pulse repetition rate and energy. The minimum value (1.1×10^{-11} cm W^{-1}) is obtained for NSs with $R_2 = 60$ nm excited with 210 nJ energy pulses at 20 Hz whereas the higher one (9.6×10^{-11} cm W^{-1}) is evaluated for NSs with $R_2 = 110$ nm excited with 408 nJ energy pulses at 200 Hz. The measured order of magnitude is in sharp contrast with the literature data reporting values ranging from -10^{-2} to -10^{-10} cm W^{-1}.[17,23] However, those data have been obtained by using laser pulse durations of nanoseconds or picoseconds and repetition rates up to 1 KHz to measure *z*-scan data on nanoparticles of different size, shape and state of aggregation. As noted above, the difference in pulse duration alone can justify order of magnitude differences in the obtained β values since different processes, occurring in the time scale of the laser pulse, are probed. Add to this, the possible occurrence of thermal effects with nanosecond pulses or at high repetition rates and the marked discrepancies with the literature data, cannot come as a surprise.

In trying to identify data that are more significant to extract reliable β values for NSs excited at 806 nm, we selected those measured at 20 Hz for NSs with $R_1 = 95$ nm; $R_2 = 110$ nm because of the regular shape of the sample and the minimization of possible thermal effects. The estimated β values are shown in Fig. 7 as a function of pulse energy. One notices a significant increase of the absolute value of (negative) β with increasing pulse energy. This is, in itself, evidence of the fact that third-order processes, assumed as the only responsible of the nonlinear transmission in the Sheik–Bahae model, are not sufficient to account for the observed behavior.

Consideration of the excitation processes that can take place in gold and contribute to the NL absorption of at 806 nm (1.54 eV) allows us to propose a simplified, tentative explanation. The nonlinear propagation equation including a term of order higher than that originating from the third order response reads

$$\frac{dI}{dz} = -\alpha I - \beta I^2 - \gamma I^3 \qquad (2)$$

In order to account for saturation effects, eqn (2) should be coupled with rate equations describing the evolution, during the pulse duration, of the electron distribution within an energy range spanning from 1.54 eV below to 1.54 eV above the Fermi level, E_F. This phenomenon has been recently described by Guillet *et al.*[41] They used the Botlzmann equation to determine the dynamics of the energy distribution function for sp electron of energy E_{sp}. This study reveals that for pulses with a duration of few hundreds femtoseconds the understanding of the third-order optical properties of metal nanoparticles requires to take into account the nonistantaneous thermalization of the conduction-electron gas (the electron thermalization is reached in more than 500 fs). Moreover, using photons with 1.5 eV energy, the light pulse only induces intraband transitions within the sp conduction band and this implies that the hot electron mechanism is the dominant contribution to nonlinear saturable absorption as compared with the interband one.[41] Furthermore, a dependence of the imaginary part of the third order susceptibility Im $\chi_m^{(3)}$ on the intensity of the laser beam (for intensities higher than 10^6 W cm^{-2}) is also predicted by the model, which is nicely confirmed by our experimental results.

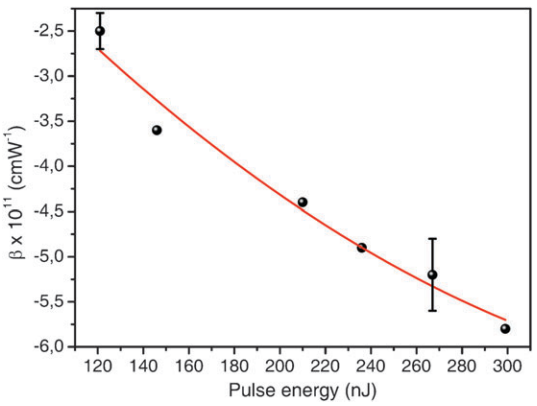

Fig. 7 Estimated β values for $R_2 = 110$ nm nanoshells in solution as a function of pulse energy.

Conclusions

Nonlinear optical response of different NSs in solution have been measured by the *z*-scan technique using 170 fs pulses at different repetition rates within a controlled pulse energy range from 120 to 500 nJ.

The data were fitted with the Sheik–Bahae model and yielded an effective value of the NL absorption coefficient β ranging between -1.1×10^{-11} and -9.6×10^{-11} cm W^{-1}, dependent on the pulse energy and repetition rate. In fact, the absolute value of the NL absorption coefficient increases both with energy and pulse repetition rate. The effect of increasing the repetition rate is likely related to thermal effects, also confirmed by an increase of the beam waist radius used for fitting the *z*-scan data.

The measured *z*-scan curves show evidence indicating that femtosecond laser pulses cause reshaping of the NSs gold coverage but the damage extent is not so large as to compromise the NSs nonlinear optical response.

Through a careful choice of the experimental conditions, we have been aimed at obtaining parameter values pertaining to the electronic contribution to the NL absorption of Au NSs unaffected by thermal or other energy relaxation effects. However, as the investigated process depends on a complicated balance of many factors, the reported figures for the NL absorption coefficient should be taken as a representative value appropriate for the specific nanostructures and excitation conditions considered here.

Acknowledgements

The authors thank Professor G. Mistura and Dr C. Semprebon for contact angle measurements. Financial support from the Italian Ministry for Education, University and Research (MIUR) through the PRIN 2007 project "Plasmonic nanostructures and their interaction with chromophores: towards innovative photonic devices and optical sensors" and from the Italian Interuniversity Consortium for Science and Technology of Materials (INSTM) through the PROMO Programme is gratefully acknowledged.

References

1 E. Hutter and J. H. Fendler, *Adv. Mater.*, 2004, **16**, 1685–1706.
2 M. E. Stewart, C. R. Anderton, L. B. Thompson, J. Maria, S. K. Gray, J. A. Rogers and R. G. Nuzzo, *Chem. Rev.*, 2008, **108**, 494–521.
3 C. Hägglund, M. Zäch and B. Kasemo, *Appl. Phys. Lett.*, 2008, **92**.
4 H. Wang, D. W. Brandl, P. Nordlander and N. J. Halas, *Acc. Chem. Res.*, 2007, **40**, 53–62.
5 S. Link and M. A. El-Sayed, *J. Phys. Chem. B*, 1999, **103**, 8410–8426.
6 K. L. Kelly, E. Coronado, L. L. Zhao and G. C. Schatz, *J. Phys. Chem. B*, 2003, **107**, 668–677.
7 C. Noguez, *J. Phys. Chem. C*, 2007, **111**, 3806–3819.
8 S. J. Oldenburg, R. D. Averitt, S. Westcott and N. J. Halas, *Chem. Phys. Lett.*, 1998, **288**, 243–247.
9 L. R. Hirsch, A. M. Gobin, A. R. Lowery, F. R. Tam, R. A. Drezek, N. J. Halas and J. L. West, *Ann. Biomed. Eng.*, 2006, **34**, 15–22.
10 S. Kalele, S. W. Gosavi, J. Urban and S. K. Kulkarni, *Curr. Sci.*, 2006, **91**, 1038–1052.
11 A. M. Gobin, M. H. Lee, N. J. Halas, W. D. James, R. A. Drezek and J. L. West, *Nano Lett.*, 2007, **7**, 1929–1934.
12 C. S. Levin, S. W. Bishnoi, N. K. Grady and N. J. Halas, *Anal. Chem.*, 2006, **78**, 3277–3281.
13 J. Kundu, F. Le, P. Nordlander and N. J. Halas, *Chem. Phys. Lett.*, 2008, **452**, 115–119.
14 W. Wenseleers, F. Stellacci, T. Meyer-Friedrichsen, T. Mangel, C. A. Bauer, S. J. K. Pond, S. R. Marder and J. W. Perry, *J. Phys. Chem. B*, 2002, **106**, 6853–6863.
15 H. I. Elim, J. Yang, J. Y. Lee, J. Mi and W. Ji, *Appl. Phys. Lett.*, 2006, **88**, 083107.
16 E. L. Falcão-Filho, C. B. De Araújo and J. J. Rodrigues, *J. Opt. Soc. Am. B*, 2007, **24**, 2948–2956.
17 Y. Gao, X. Zhang, Y. Li, H. Liu, Y. Wang, Q. Chang, W. Jiao and Y. Song, *Opt. Commun.*, 2005, **251**, 429–433.
18 D. D. Smith, G. Fischer, R. W. Boyd and D. A. Gregory, *J. Opt. Soc. Am. B*, 1997, **14**, 1625–1631.
19 R. Philip, G. R. Kumar, N. Sandhyarani and T. Pradeep, *Phys. Rev. B: Condens. Matter Mater. Phys.*, 2000, **62**, 13160–13166.
20 W. Wang, Y. Wang, Z. Dai, Y. Sun and Y. Sun, *Appl. Surf. Sci.*, 2007, **253**, 4673–4676.
21 G. Piredda, D. D. Smith, B. Wendling and R. W. Boyd, *J. Opt. Soc. Am. B*, 2008, **25**, 945–950.
22 Q. Qu, Y. Zhang, H. Li, J. Qiu and C. Zhu, *Opt. Mater.*, 2006, **28**, 259–265.
23 S. Matsubara, T. Hayakawa, J. Yang, M. Nogami, S. Okamoto and N. Koshikawa, *J. Phys. Chem. C*, 2008, **112**, 13917–13921.
24 N. Rotenberg, A. D. Bristow, M. Pfeiffer, M. Betz and H. M. Van Driel, *Phys. Rev. B: Condens. Matter Mater. Phys.*, 2007, **75**, 155426.
25 J. M. Lamarre, F. Billard, C. H. Kerboua, M. Lequime, S. Roorda and L. Martinu, *Opt. Commun.*, 2008, **281**, 331–340.
26 V. Prasad, A. Mikhailovsky and J. A. Zasadzinski, *Langmuir*, 2005, **21**, 7528–7532, DOI: 10.1021/la051036d.
27 C. M. Aguirre, C. E. Moran, J. F. Young and N. J. Halas, *J. Phys. Chem. B*, 2004, **108**, 7040–7045.
28 T. Pham, J. B. Jackson, N. J. Halas and T. Randall Lee, *Langmuir*, 2002, **18**, 4915–4920.
29 W. Stober, A. Fink and E. Bohn, *J. Colloid Interface Sci.*, 1968, **26**, 62.
30 D. G. Duff, A. Baiker and P. P. Edwards, *Langmuir*, 1993, **9**, 2301–2309.
31 G. Gotesman and R. Naaman, *Langmuir*, 2008, **24**, 5981–5983.
32 D. F. Siqueira Petri, G. Wenz, P. Schunk and T. Schimmel, *Langmuir*, 1999, **15**, 4520–4523.
33 M. Sheik-Bahae, A. A. Said, T. Wei, D. J. Hagan and E. W. Van Stryland, *IEEE J. Quantum Electron.*, 1990, **26**, 760–769.
34 A. Van Blaaderen and A. P. M. Kentgens, *J. Non-Cryst. Solids*, 1992, **149**, 161–178.
35 J. H. Kim, W. W. Bryan and T. Randall Lee, *Langmuir*, 2008, **24**, 11147–11152.
36 M. R. Rasch, K. V. Sokolov and B. A. Korgel, *Langmuir*, 2009, **25**, 11777–11785.
37 T. C. Preston and R. Signorell, *ACS Nano*, 2009, **3**, 3696–3706.
38 S. Link and M. A. El-Sayed, *Int. Rev. Phys. Chem.*, 2000, **19**, 409–453.
39 O. L. Muskens, N. Del Fatti and F. Vallée, *Nano Lett.*, 2006, **6**, 552–556.
40 P. Park, M. Pelton, M. Liu, P. Guyot-Sionnest and N. F. Scherer, *J. Phys. Chem. C*, 2007, **111**, 116–123.
41 Y. Guillet, M. Rashidi-Huyeh and B. Palpant, *Phys. Rev. B: Condens. Matter Mater. Phys.*, 2009, **79**, 045410.

